PHASE FUNCTIONS OF DEEP-SPACE ORBITAL DEBRIS

M.D. Hejduk
AFSPC/A9L

ABSTRACT

Because most work on deep-space orbital debris has been in the form of debris surveys, relatively little effort has been directed to the photometric characterization of these debris objects. The present abundance of well-calibrated GEODSS satellite photometric data, however, can enable the beginnings of such an investigation. The brightness versus phase response of some 250 debris objects was studied and compared to the response for approximately 1000 payloads and 750 rocket bodies. Debris brightness response remains better circumscribed than that for payloads or rocket bodies, but with increased "retrograde" brightness-vs-phase behavior. Straight-line brightness versus phase response, typical for most payloads and rocket bodies, is not nearly so prevalent for debris but still constitutes the substantial majority of the debris cases. For brightness prediction, a straight-line phase function is a better predictor than the diffuse sphere approximation in about 80% of the cases, a figure similar to that for the other object types.

With the general behavior of the debris objects characterized, such objects were subdivided into three broad response categories, with further subdivisions into a total of nine categories, as a function primarily of the linear slope (or lack thereof) of the phase function and the spread about the fit line (or mean value). The categories were assigned by visual examination of brightness-versus-phase-angle plots, and the goal was to determine statistical quantities that could reliably separate both the larger and smaller categories. Fitted slope is a poor discriminator and *t*-test p-value a substantially better one, but the p-value at which discrimination is most reliable is much smaller than what would generally be used for hypothesis testing. Statistical discrimination among the smaller sub-categories is much less successful, but some of the natural groupings of the results are surprising.

1. DATASET

The Ground-based Electro-Optical Deep-Space Surveillance (GEODSS) sensing system comprises three USAF optical sites (Socorro, NM; Maui, HI; and Diego Garcia, BIOT), each containing three 1-m class telescopes deployed for the surveillance of artificial satellites. In 2004 and 2005, all of these telescopes were upgraded from tube- to CCD-based cameras; and with this upgrade the systems were able to collect, record, and store calibrated photometry as part of each metric measurement. A typical metric track consists of an open-aperture, sidereal-mode collection of two streaks, each the product of a metrically- and photometrically-calibrated frame. In-frame photometric calibration consists of a solution against registration stars that have been pre-selected to be solar-equivalent; a typical solution would include 3-10 such stars. This procedure is believed to produce photometry good to three-tenths of a visual magnitude. Because the photometric results for the two streaks of a metric collection differ very little, they are usually averaged to produce a single photometric measurement, phase angle (here defined as the sun-satellite-sensor angle, with 0 phase indicating opposition and 180 degrees a completely unilluminated situation), and observing range for the particular track. The present GEODSS system limits its tracking response to phase angles less than 105 degrees.

Since these telescopes are high-throughput, the photometry collected since 2004 may well represent the largest satellite photometry repository in existence, with over 1.7 million track-averaged measurements. Fig. 1 shows the number of catalogued objects on which appreciable data exist, either to permit a full-phase brightness solution (*ca.* 30 measurements) or an analysis-grade investigation of the phase function (100 measurements). Fig. 2 provides a CDF plot of the number of track-averaged brightness measurements collected per object, broken out by object type. For most of the cases (some 80%), payloads and rocket bodies receive close to the same collection rate, with some payloads obviously exceeding this. Collection rates for debris objects consistently lag that for payloads and rocket bodies, often significantly; however, most objects still meet the 100-measurement analysis-enabling threshold.

The NORAD-published satellite catalogue gives basic debris object pedigree: for example, the international designator and common name assigned to debris objects indicate whether the object originated from a payload or rocket body. A NASA database provides even more pedigree information by tracing each deep-space debris object that has arisen from on-orbit fragmentation to a particular break-up event and type. While this pedigree information was not explicitly employed in the present study, once the behavior of debris objects *simpliciter* is understood, the next logical step is to look for correlation between photometric behavior and a particular type of debris pedigree.

Fig. 1: Objects Analyzed by Object Type

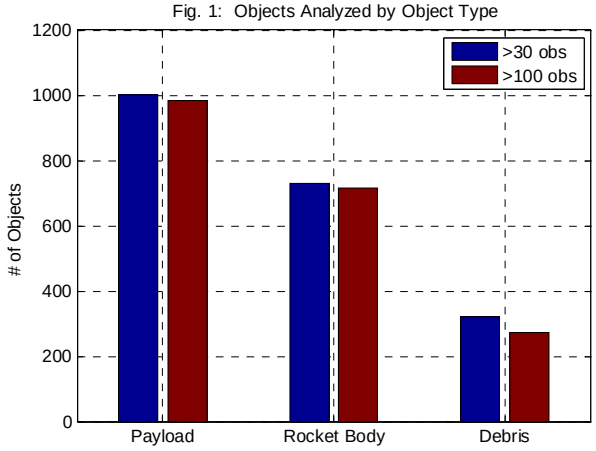

Fig. 2: # of Measurements by Object Type

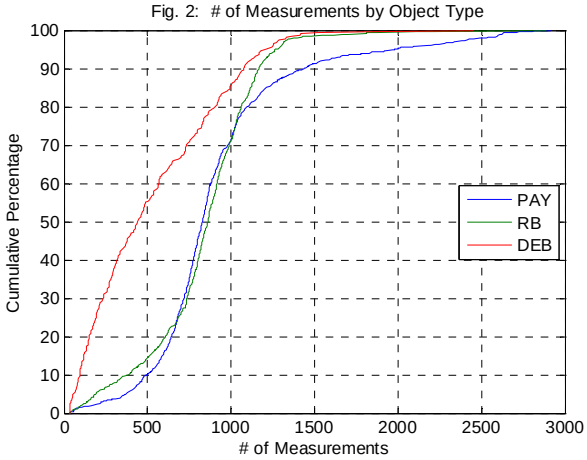

2. BINNING BRIGHTNESS RESPONSE

Phase-function characterization will ultimately result, one hopes, in an analytic curve or family of curves of resultant brightness versus solar phase angle; and to achieve this, curve-selection and fitting techniques will need to be applied to individual datasets. One must determine whether each dataset is to be evaluated *en masse* or should be first collected into phase-angle bins of appropriate size, with the averaged value for each bin serving as the representative data point; and the proper procedure is not initially obvious. Since a characterization of the phase function for the entire expected phase range (0-105 degrees) is desired, binning initially appears preferable in order to ensure that resultant curve-fits not be predominated by those phase regions that merely happen to be heavily sampled; on the other hand, individual bins themselves can often be undersampled and therefore affect the resultant fit disproportionately. The hope is that the results from both approaches will be similar enough that for the present analysis the question will not assume much importance.

The employed binning scheme was to use ten-degree phase bins, representing each by the median value of the encapsulated data and the midpoint phase angle (*e.g.,* a bin of 0-10 degrees would be represented by the median of brightness values with phase angles between 0 and 10 degrees, and would be associated with a phase angle value of 5 degrees. With such binning imposed on each object's dataset, one can immediately attempt an initial notional characterization of the phase brightness effect among different object times by examining the brightness difference between the first (0-10 degrees) and the penultimate (80-90 degree) bins, and these data are reported as CDF plots in Fig. 3.

Fig. 3: Phase Brightness Differences by Object Type: Obs>100

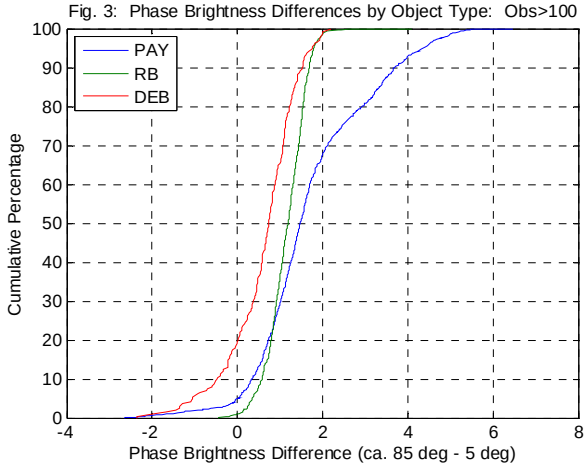

The differences among the three object types are obvious. Payloads almost never produce any "reverse-phase" or "retrograde" brightness behavior—that is, an

increasing brightness with the reduced illumination of higher phase angle; and a notable percentage exhibit a very large brightness difference with phase angle: 20% of the cases present a brightness difference larger than 3 Mv. Rocket bodies show a much more modest dependence on phase angle, with all such variation confined to a 2 Mv spread and very few retrograde situations. It is presumed that the cylindrical shape produces a highly-variable aspect function, giving rise to a scattered brightness response that will depend on phase angle much more weakly. Similar behavior is observed here with debris, although a specular component is not (yet) presumed. The amount of retrograde behavior, nearly 20% of the cases, is unexpected. The number of such cases for which the retrograde result is legitimate rather than merely an artifice of binning remains to be investigated.

3. EXPLORATORY CURVE FITTING

The next exploratory step is to determine whether, at the aggregate level, some simple curve-fits appear to serve well to explain and model the observed high-vs-low-phase brightness differences. If a particular functional form appears promising, perhaps it can serve as a discriminator in attempting to determine the different types of phase response that space debris present. Numerous previous studies [1 2 3 4 5] have indicated that the brightness-vs-phase response for payloads is modeled well by straight lines, so the first fit-type to attempt is a simple straight-line, least-squares fit. Experience with attempting simple, binned brightness-vs-phase fits to enable brightness prediction and therefore probability of detection for sensor tasking [6 7] have indicated that outlying bins can present a fit problem and therefore counsels a more robust technique, such as robust regression; the method employed here uses the (iteratively-reweighted) bisquare cost function. Finally, although the purpose of this particular paper is not to pass a durable judgment on the use of the diffuse sphere approximation for debris, this approach is so widely used in so many areas of satellite photometric analysis that it should be included here also. The diffuse sphere brightness prediction typically used is of the form

$$Mv = -26.74 - 2.5\log_{10}(A\alpha F(\varphi)) + 5.0\log_{10}(R) \tag{1}$$

For which A is the target's cross-sectional area, α is the target's albedo, R is the distance from the observer to the target, and the phase function $F(\varphi)$ is defined as

$$F(\varphi) = \frac{2}{3\pi^2}\left[(\pi - \varphi)\cos\varphi + \sin\varphi\right], \tag{2}$$

with φ, the solar phase angle, in radians. If the target characteristics are explicitly known (*i.e.,* cross-sectional area and albedo), then the target brightness can be calculated explicitly. As typically neither of these two quantities is known, the brightness curve is fitted to the data through a nonlinear least-squares determination of the albedo-area product ($A\alpha$); once this product is determined, then an assumed value for the target albedo can allow a calculation of target size.

Fig. 4: t-test Fit Results for Linear LSQ: Binned/Unbinned Fits (p=0.05)

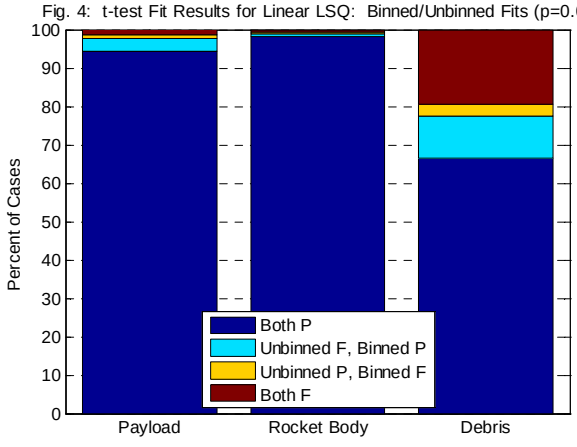

Fig. 5: t-test Fit Results for Linear LSQ: Binned/Unbinned Fits (p=0.01)

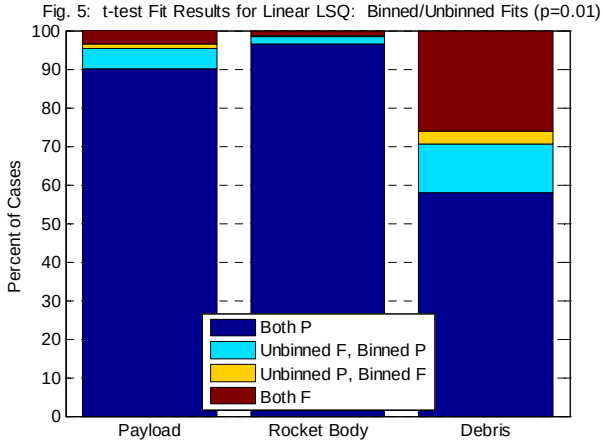

The first question to address is the observed differences in curve-fit success as a function of whether the datasets are binned or unbinned. This question was investigated with respect to the straight-line least-squares and robust regression fits, with "success" determined by a successful *t*-test against the single regressor variable. Figs. 4 and 5 present two sets of results, the first for a *t*-test p-value of 0.05 and the second for a value of 0.01. The red area indicates the percentage of cases in which both the binned and unbinned datasets fail the t-test; the yellow those cases in which the binned fit fails but the unbinned passes; the aqua those cases in which the unbinned fit fails but the binned passes; and the dark blue those cases in which both fits pass. It should be stated in advance that the smaller number of points in the binned fits (ten points, one corresponding to each of the bins) will generally produce better *t*-test results, so a significant improvement in the success rate of binned fits is necessary in order to conclude that it is the superior paradigm. One is struck immediately by both approaches' degree of success for payloads and rocket bodies; linear fits are likely to be of considerable value in characterizing brightness response for these object types. The results for debris are somewhat less sanguine in that for 25% of cases the linear fit is of no statistical significance and that binned response outperforms full-sample response for about 10% of debris satellites. However, *t*-test failures may indicate that such cases are best characterized by simply using the mean or median brightness (these cases will need to be examined visually to determine whether the data distribution shows no systematic variation with brightness); and the superior performance of the binned fits is not great enough indicate a significant difference between the two approaches; indeed, it should be sufficient to proceed with whichever approach is more convenient for the analysis.

Figs. 6 and 7 compare the performance of traditional linear LSQ fitting to robust regression. The areas of interest in this graph are the aqua and yellow regions—those where one technique succeeds and the other fails. As can be seen, at both p-levels surveyed the aqua-yellow regions are very small, 5% or fewer of the cases. The conclusion therefore is that either the linear LSQ or robust regression techniques are adequate for the present analysis, as they produce nearly the same results.

Fig. 6: t-test Fit Results for Linear LSQ vs Robust Fit (p=0.05)

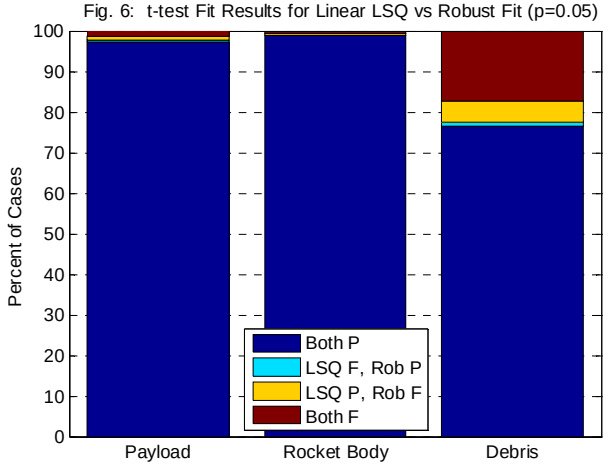

Fig. 7: t-test Fit Results for Linear LSQ vs Robust Fit (p=0.01)

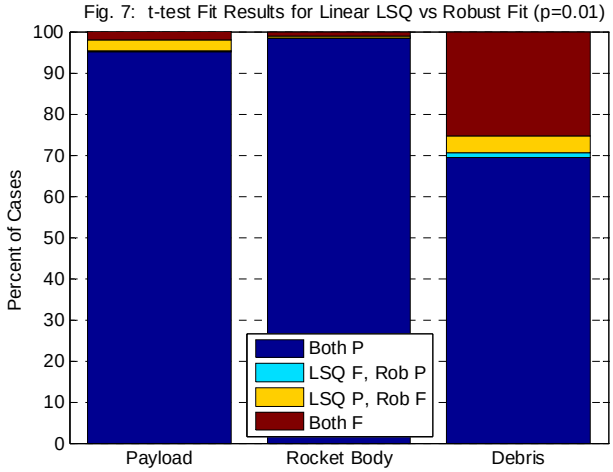

Finally, a quick comparison of straight-line fits versus the diffuse-sphere curve family is in order. Least-squares fitting was used for both fit-types (non-linear in the latter case), and the RMS values from both fits were compared. Fig. 8 shows that when the *t*-test passes for the linear fit, this fit outperforms the diffuse-sphere fit about 85% of the time—a significant finding; curiously, for the case of rocket bodies, such performance falls to 75%. When the t-test fails, the outperformance is in nearly every case; but all this result actually reveals is that any curve-fitting for such cases is likely to be futile. Fig. 9 characterizes the RMS differences (for both passed and failed t-tests) between the two approaches. As previous studies have shown, payloads resist the diffuse-sphere approximation the most strongly; the surprise is how much more closely rocket bodies embrace it. Debris falls between these two extremes; and its overall RMS difference—less than 0.1 Mv for about 80% of the cases—does not show a fundamental conceptual superiority. Whether the diffuse sphere approximation is adequate for size estimation is a question left for another study; what can be said here is that for the (more modest) purposes of brightness prediction, straight-line fits (or median approximation where appropriate) are a superior fitting technique in the substantial majority of cases.

Fig. 8: Linear RMS < Diffuse Sphere RMS

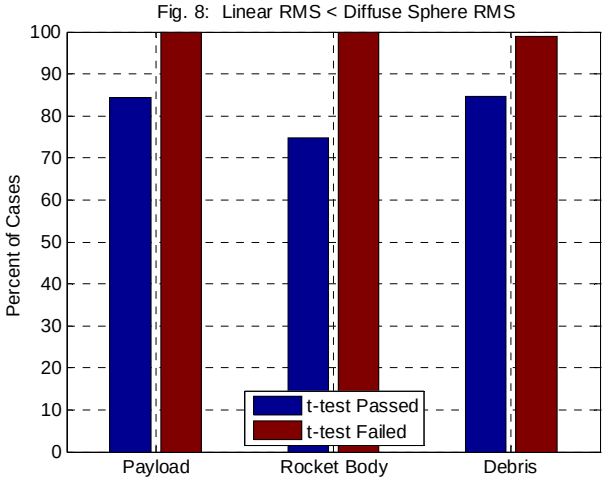

Fig. 9: Diffuse Sphere RMS - Linear LSQ RMS (Unbinned Data)

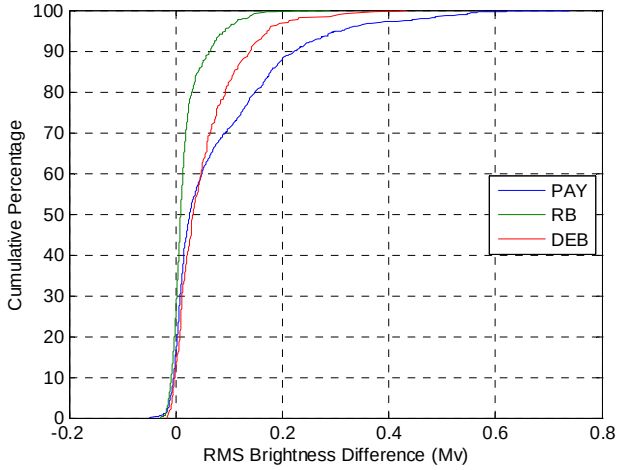

4. PHASE RESPONSE CASE CONSIDERATION

The exploratory portions of the analysis have revealed the broad categories into which phase-brightness response for debris is likely to divide itself: a moderate to strong "prograde" brightness dependence on phase, probably conforming reasonably well to a straight-line model; little to no brightness dependence on phase; and a "retrograde" dependence on phase in which brightness actually increases with increased phase angle. The initial screening of brightness versus phase scatter-plots has suggested further subdividing these broader categories to consider brightness spread and outlier characteristics. The result is nine categories, as defined in Table 1 and represented by actual example in Fig. 10. To keep this paper publicly releasable, no satellite identification numbers are used; and the brightness axis is normalized by subtracting the brightest measurement's value from the entire dataset.

Table 1: Definition of Debris Brightness versus Phase Response Bins/Categories

Type	Title	Definition
1	Blob, range > 3 Mv	The dataset presents no systematic brightness variation with phase angle, and the overall spread of brightness values exceeds 3 Mv
2	Blob, 2 Mv > range > 3 Mv	The dataset presents no systematic brightness variation with phase angle, and the overall spread of brightness values lies (mostly) between 2 and 3 Mv
3	Blob, 1 Mv > range > 2 Mv	The dataset presents no systematic brightness variation with phase angle, and the overall spread of brightness values lies (mostly) between 1 and 2 Mv
4	Prograde slope; appreciable dim outliers	The dataset presents a more or less linear brightness variation with phase angle, with the addition of notable outliers on the dim side of the fit line
5	Prograde slope; appreciable bright outliers	The dataset presents a more or less linear brightness variation with phase angle, with the addition of notable outliers on the bright side of the fit line
6	Prograde slope; wide spread	The dataset presents a more or less linear brightness variation with phase angle. Outliers are distributed evenly on both sides of the fit line, and the spread about the fit line exceeds ±1 Mv more than just occasionally
7	Prograde slope; narrow spread	The dataset presents a more or less linear brightness variation with phase angle. Outliers are distributed evenly on both sides of the fit line, and the spread about the fit line remains within ±1 Mv for nearly all points
8	Retrograde slope; wide spread	To the degree that the dataset presents a systematic variation with slope, this variation is in the unexpected direction of increased brightness with increased phase angle; and spread about the fit line (which may fail the *t*-test) is generally broader than ±1 Mv
9	Retrograde slope; narrow spread	To the degree that the dataset presents a systematic variation with slope, this variation is in the unexpected direction of increased brightness with increased phase angle; and spread about the fit line (which passes the *t*-test) is generally within ±1 Mv

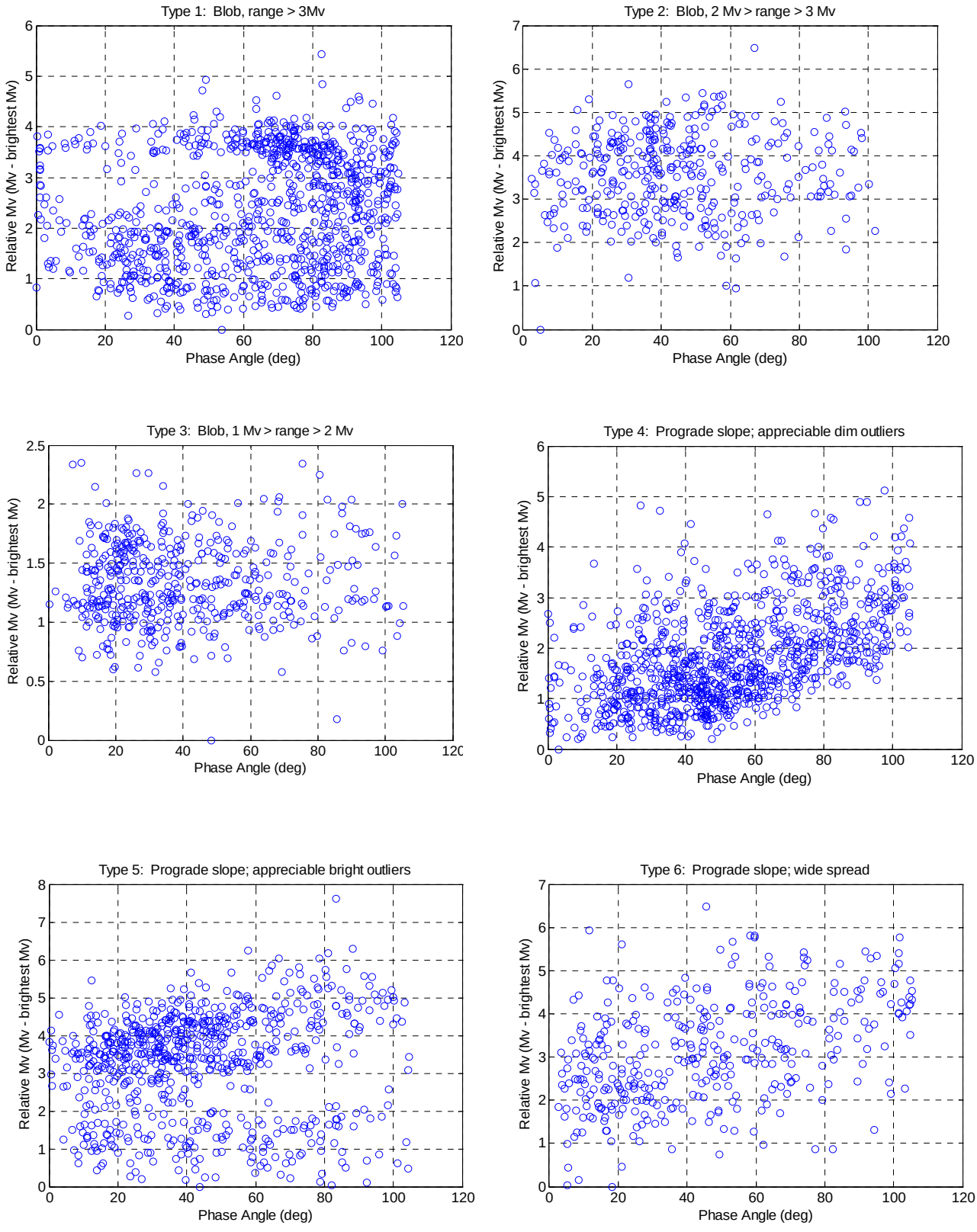

Fig. 10: Example plots of the nine phase response types

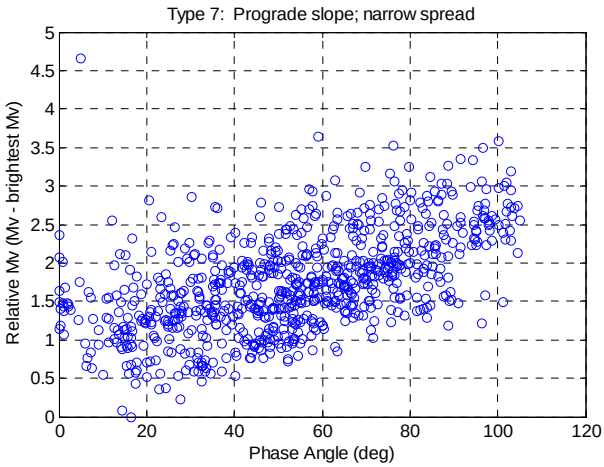

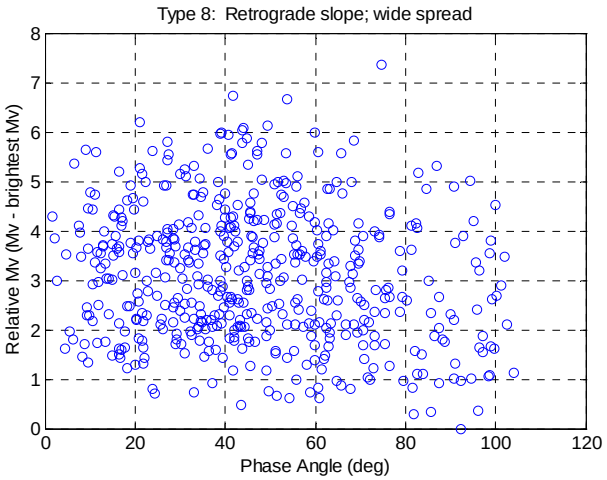

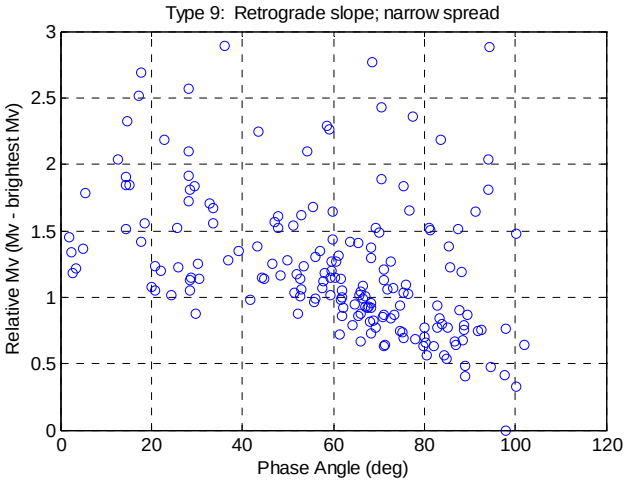

Just over 300 debris brightness-vs-phase plots were manually examined and placed into one of these nine categories. There is, to be sure, a certain level of arbitrariness in this categorization, especially when outlier characteristics are being assessed by eye; but this is the best way to get an overall sense of more specific brightness-phase behavior and to begin to align human pattern discernment with the results of specific statistical tests. Table 2 provides frequency-of-occurrence data for each of the three broader categories (blob, prograde slope, retrograde slope) and each of their subcategories. The majority of cases are of the prograde type; and 40% of these (25% of the overall sample) are well-defined linear-response situations with nearly all data within 1 Mv of the fit line. Just over 30% are of the blob type, for which no curve fit is likely to be successful or illuminating. A very small number—only a little over 5%—are of the retrograde type, and only one quarter of these (1.5% of the overall total) follow the fit line tightly and therefore convincingly. It thus seems that one can categorize debris phase functions to be roughly two-thirds linear response with phase (nearly all of which is prograde) and one-third invariant "blob" response with phase. To be sure, it is possible that there may be some other functional form that could provide a better fit to the brightness data that does exhibit dependence on phase angle; but no other functions suggested themselves to the present author during this manual review of brightness-versus-phase scatter plots.

Table 2: Frequency of Occurrence for Debris Phase-Response Categories

Category	% of all Cases	Sub-Category	% of Sub-Category	% of all Cases
Blob	31.6%	Blob, range > 3 Mv	60.5%	19.1%
		Blob, 2 Mv > range > 3 Mv	25.6%	8.1%
		Blob, 1 Mv > range > 2 Mv	14.0%	4.4%
Prograde Slope	62.1%	Prograde slope; appreciable dim outliers	22.5%	14.0%
		Prograde slope; appreciable bright outliers	5.9%	3.4%
		Prograde slope; wide spread	32.0%	19.9%
		Prograde slope; narrow spread	39.6%	24.6%
Retrograde Slope	6.3%	Retrograde slope; wide spread	76.5%	4.8%
		Retrograde slope; narrow spread	23.5%	1.5%

If the morphology shown above is accepted, then what is important is to be able to separate the different canonical types by statistical test so that for any given situation the proper predictor function can be selected, without the need to review results manually. One possible separator is the fitted slope, as it may well be that the larger slopes are associated with the prograde linear cases and the smaller slopes with the invariant "blob" cases. Fig. 11 provides CDF plots of fitted slopes for the three principal response types. If the three CDF curves overlapped only very little, then this parameter might be able to function as a useful discriminator; as it is, 40% of the prograde slope CDF overlaps with about 60% of the invariant "blob" CDF; so this factor will not be helpful in discriminating between the two cases that compose 95% of the debris objects.

Fig. 11: Debris Category vs Fitted Slope

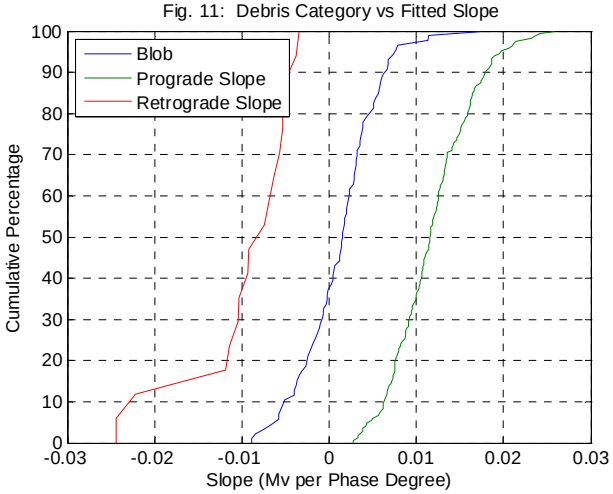

Fig. 12: Debris Category vs t-test Result

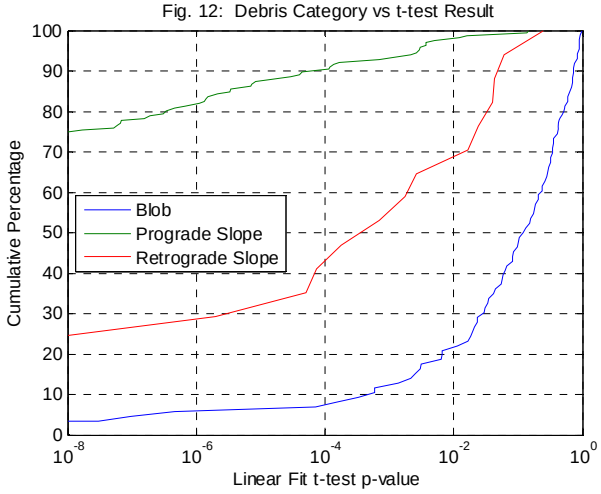

Fitted slope was investigated first as a discriminator because of its immediate relationship to a viewable graph, giving it an intuitive appeal; but greater success might in any case have been expected from the *t*-test p-value, as this relates directly to the determinateness of the fit. Fig. 12 provides a CDF plot against this factor, and one finds immediately an improved situation. The "blob" line shows a notably increased curvature beyond the 10^{-4} point, and at this point one has accounted for 90% of the prograde slope cases while including less than 10% (closer to 8%) of the blob cases. The retrograde slope cases can be eliminated by examining the actual fitted slope values. One can thus recommend using a *t*-test p-value of 10^{-4} to separate invariant from prograde sloped response. One should note that this p-value is two orders of magnitude smaller than that which would typically be used to reject the null hypothesis in analysis of variance or other hypothesis-testing approaches.

Fig. 13: Debris Category vs Fitted Slope

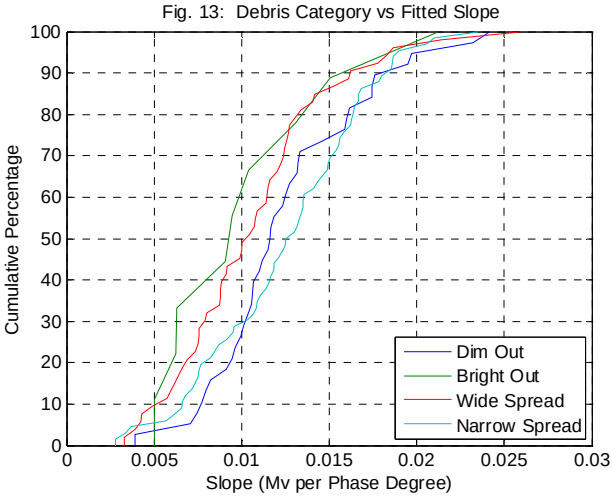

Fig. 14: Debris Category vs t-test Result

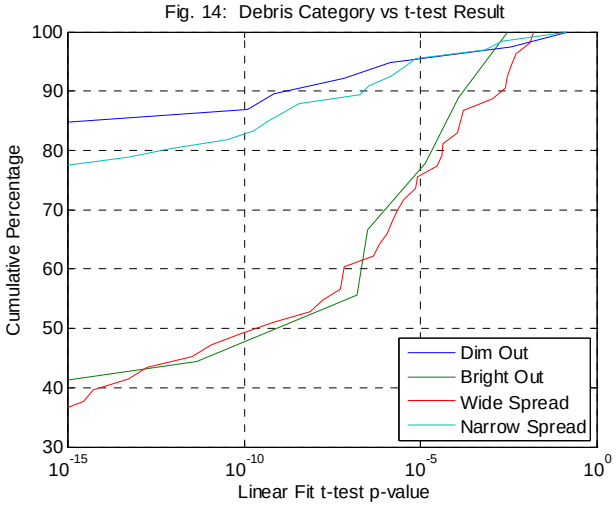

Finally, one wishes to determine whether either of these separation criteria is effective to differentiate among the four individual species of the prograde slope genus. Fig. 13 below shows a CDF for each of these four species

against fitted slope, and it is clear that this parameter is no more successful a sorting criterion here than it is among the three genius of debris generally. Drawing from earlier success, fig. 13 more hopefully attempts this separation against the *t*-test value. At a gross level, there is perhaps some separation power at values of *ca.* 10^{-15}, which would identify about 80% of two of the four species and only 40% of the other two; but this level of performance is not particularly impressive; it is certainly not strong enough to function as a durable discriminator. The graph does, however, reveal a curious similarity between the narrow spread case and that of dim outliers, and the wide-spread case and that of bright outliers. Dim outliers clearly affect the determinacy of the fit much less severely than do bright outliers, apparently because these dim-outlier cases possess fewer such outliers, each of which is also less extreme. Specular response, which is presumed to be the cause of bright outliers, produces both more pervasive and severe bright measurements.

5. CONCLUSION AND FUTURE WORK

Debris objects do indeed have different photometric properties from other spacecraft types, as they appear to fall between the large phase-induced brightness differences of the more stable and complex payloads and the much more circumscribed aspect-dominated response of rocket bodies. That said, the straight-line phase function so well documented for payloads is still useful, although there is a greater number of cases that cannot sustain it; but in the substantial majority of situations it outperforms the diffuse sphere approximation as a brightness predictor. Debris objects separate themselves into three main categories ("blob, prograde slope, and retrograde slope), and the least-squares linear fit *t*-test p-value of 10^{-4} is a good separator among these categories. No obvious separation factors among the sub-categories of each of the three main divisions suggested themselves.

Two continuation activities of this study are planned. First, deep-space debris objects will be separated by those known to have arisen from a fragmentation event and those that have not, as well as the different fragmentation event types, to determine if their overall photometric properties differ among these groups and therefore if photometry is useful to distinguish among them. Second, for those debris objects for which there are acceptably-large samples of photometric and radar cross-section (RCS) data, object sizes will be estimated from the NASA size estimation model (SEM) and the diffuse-sphere approximation and these two results sets compared statistically. While the photometrically-derived size solution is expected to be the less reliable, nonetheless it will be useful to establish how it can emulate the RCS-derived size estimates, perhaps as a helpful supplement for those situations for which no RCS data are available.

6. REFERENCES

1. Lambert, J.V., "Interpretation of Geosynchronous Satellite Phase Angle versus Magnitude Relationships", Contract F05603-90-C-0010 Specialized Data Report: MOTIF FY95-01, 30 NOV 1994.

2. Lambert, J.V., "Analysis of Magnitude versus Phase Angle Data for Two Classes of Deep Space Satellites", Contract F05604-95-C-9011 Specialized Data Report: MSSS FY96-04, 11 OCT 1996.

3. Lambour, R.L., "Phase Angle Dependence of Satellite Brightness Derived from Space-Based Visible Data", MIT/LL Project Report SPC-8, 20 FEB 2001.

4. Hejduk, M.D., Kervin, P.W., Lambert, J.V., Stansbery, E.G., Africano, J.L, and Pearce, E.C., "Visual Magnitude Satellite Catalogue Release 1.0", 2001 AMOS Technical Conference, Maui HI, SEP 2001

5. Lambour, R.L. and Sayer, R.W., "ETS Measurements of Satellite Phase Curves at High Phase Angles", MIT/LL Project Report ETS-138, 12 SEP 02.

6. Okada, J.M. and Hejduk, M.D. "Satellite Brightness Estimation using Kriging Optimized Interpolation." 2005 AMOS Technical Conference, Kihei, HI. September 2005

7. Hejduk, M.D. "Approaches to Satellite Characterization: the Deterministic/Stochastic Divide." American Statistical Association Conference on Quantitative Methods and Statistical Applications in Defense and National Security, Santa Monica, CA. February 2006.